


Morphological, biochemical and mechanical properties of articular cartilage and subchondral bone in rat tibial plateau are age related

Pengling Ren,¹ Haijun Niu,¹ He Gong,¹  Rui Zhang¹ and Yubo Fan^{1,2}

¹Key Laboratory for Biomechanics and Mechanobiology of Ministry of Education, School of Biological Science and Medical Engineering, Beihang University, Beijing, China

²National Research Center for Rehabilitation Technical Aids, Beijing, China

Abstract

The purpose of this study was to investigate age-related changes in the morphological, biochemical and mechanical properties of articular cartilage (AC) and subchondral bone in the rat tibial plateau. Female Wistar rats were grouped according to age (1, 3, 5, 7, 9, 11, 13, 15, 16 and 17 months, with 10 rats in each group). The ultrastructures, surface topographies, and biochemical and mechanical properties of the AC and subchondral bone in the knee joints of the rats were determined through X-ray micro-tomography, histology, immunohistochemistry, scanning electron microscopy (SEM), atomic force microscopy and nanoindentation. We found that cartilage thickness decreased with age. This decrease was accompanied by functional condensation of the underlying subchondral bone. Increased thickness and bone mineral density and decreased porosity were observed in the subchondral plate (SP). Growth decreased collagen II expression in the tibial cartilage. The arrangement of trabeculae in the subchondral trabecular bone became disordered. The thickness and strength of the fibers decreased with age, as detected by SEM. The SP and trabeculae in the tibial plateau increased in roughness in the first phase (1–9 months of age), and then were constant in the second phase (11–17 months of age). Meanwhile, the roughness of the AC changed significantly in the first phase (1–9 months of age), but the changes were independent of age thereafter. This study gives a comprehensive insight into the growth-related structural, biochemical and mechanical changes in the AC and subchondral bone. The results presented herein may contribute to a new understanding of the pathogenesis of age-related bone diseases.

Key words: articular cartilage; development; mechanical properties; microarchitecture; subchondral bone.

Introduction

Articular cartilage (AC) and subchondral bone constitute a functional unit that maintains its own integrity through its specific metabolic patterns, and this unit plays an important role in distributing load and absorbing shock. These functions can persist for decades under normal physiological conditions. However, degenerative diseases targeting AC can cause joint dysfunction, such as osteoarthritis (OA), which affects half of people over 65 years old (Bijlsma et al. 2011). Therefore, considerable effort has been devoted to studying the pathology of AC degeneration.

Articular cartilage degeneration is attributed to many factors, such as metabolism, age and overloading (Lotz & Loeser, 2012). Notably, age changes the composition, structure and mechanical properties of both the cartilage and subchondral bone (Stolz et al. 2009; Temple et al. 2009; Lories & Luyten, 2011; Lotz & Loeser, 2012; Li et al. 2015a,b). Nevertheless, the extent to which age affects these structures remains unknown. Thus, mechanisms by which the composition, structure, morphology, and mechanical properties of cartilage and subchondral bone are modified during normal growth and development should be carefully described to understand the mechanisms of cartilage degeneration.

The main components of AC include proteoglycans (PGs), type II collagen fibers and water. PGs embedded in a meshwork of collagen fibrils form the principal matrix components, which maintain the biomechanical properties of AC. PGs, which primarily exist as aggregates, are formed by a high concentration of negatively charged sulfated glycosaminoglycans (sGAGs), which maintain the expanded states and the elasticity of cartilage. Meanwhile, the

Correspondence

He Gong, School of Biological Science and Medical Engineering, Beihang University, Room 509, Yifu Building, Haidian, Beijing, China 100083. T: 86-13844801003; E: bmgonghe@buaa.edu.cn

Accepted for publication 4 November 2017
Article published online 20 December 2017

meshwork of collagen fibrils is responsible for the tensile strength of the tissue (Maroudas et al. 1980; O'Hara et al. 1990; Mow et al. 1992; Pearle et al. 2005). sGAG content decreases with age, and collagen content is also affected by age (Brama et al. 2000; Li et al. 2015a,b). The percentage of water content also significantly decreases with age (Kobayashi-Miura et al. 2016). Subchondral bone is mainly composed of collagen (15–25%), minerals (30–50%) and water (25–60%; Brama et al. 2002). The water content in the subchondral bone significantly decreases with age, whereas the contents of calcium and collagen increase with age (Brama et al. 2002; Li et al. 2015a,b).

In terms of morphology, age-related cartilage defects and fibrillation first occur in the superficial zone of AC (Armstrong & Mow, 1982; Hollander et al. 1995; Bae et al. 2003; Lotz & Loeser, 2012). For instance, the surface topography of the AC is altered during early degradation at the nanoscale (Peng & Wang, 2013). The orientation and organization of the collagen fibrils change from parallel to the articular surface to an arcade-like Benninghoff structure with age (Otsuki et al. 2008; Van Turnhout et al. 2008; Carames et al. 2012). In addition, the thickness of AC decreases with age (Hudelmaier et al. 2001). Subchondral bone comprises two distinct anatomic entities, namely, the subchondral bone plate and subchondral trabecular bone (ST; Ding et al. 2002; Li et al. 2013). The thickness and density of the subchondral bone plate increase with age. Furthermore, the thickness of AC is negatively correlated with the thickness of the subchondral bone plate, bone volume fraction (BV/TV) and trabecular thickness (Tb.Th) of the ST, and it is positively correlated with the porosity of the subchondral bone plate (Hamann et al. 2013).

Regarding mechanical properties, the elastic modulus of AC decreases with age, and its tensile strength decreases significantly (Guo et al. 2007; Lau et al. 2008; Moriyama et al. 2012). The mechanotransduction during joint movements can cause bone modeling that modifies the microstructure of the subchondral bone, which becomes stiff with aging. This effect is related to the increased mass and density, and reduced porosity of bone (Ding, 2010; Wang et al. 2013).

Age-related changes in the composition and mechanical properties of the cartilage and subchondral bone, as well as their interaction, have been explored through histopathology experiments and mechanical analysis (Ding et al. 2002; Hamann et al. 2013, 2014). Nonetheless, the results from different studies are not consistent because of intra-specimen differences, and variations in measurement conditions and research methods. To overcome these limitations, we systematically investigated age-related changes in AC and subchondral bone through multi-modal approaches. Generally, the animal models of OA are classified into two categories, namely, spontaneous or induced. A spontaneous OA-like phenotype has been found in various inbred strains of mice, guinea pigs and macaques. All these models exhibit the advantage of spontaneous disease phenotypes, but the

mechanism underlying the phenotype of some animal strains may not necessarily be the same as that of OA in humans. The major problem of these models is the individual variations in the incidence rate of OA. A rat model is unsuitable for naturally occurring age-related joint diseases, such as OA; however, old rats may develop joint diseases naturally (Loeser, 2009). Thus, female Wistar rats aged 1, 3, 5, 7, 9, 11, 13, 15, 16 and 17 months were selected to characterize the changes in the morphological, biochemical and mechanical properties in knee joints. The relationships between these age-related changes were also investigated. This study may provide new insights into the pathogenesis of age-related bone diseases.

Materials and methods

Materials

This study was performed in strict accordance with the recommendations of the Laboratory Animal Standardization Committee. The study protocol was approved by the Science and Ethics Committee of the School of Biological Science and Medical Engineering in Beihang University, China (Approval ID: 20150519). A total of 100 female Wistar rats aged 1, 3, 5, 7, 9, 11, 13, 15, 16 and 17 months ($n = 10$ /each age group) were purchased from the Experimental Animal Center of Jilin University. These rats were housed under the same conditions and provided a standard rodent diet (autoclaved NIH-31 with 6% fat; 18% protein; Ca:P, 1:1; and fortified with vitamins and minerals) and tap water. The environmental temperature was 24 ± 2 °C in natural light. Knee joints were harvested for testing (Fig. 1). Right knee joints were fixed in 4% paraformaldehyde (PFA) for 24 h and prepared for X-ray micro-tomography (XMT), as well as histological and immunohistochemistry analyses. Left knee joints were stored at -20 °C prior to atomic force microscopy (AFM), scanning electron microscopy (SEM) and nanoindentation analyses.

Methods

Measurements of bone mineral density (BMD) and microarchitecture parameters by XMT scanning

Whole knee joints were placed in the extended position during scanning in the XMT system (Skyscan 1076, Bruker, Luxembourg, Belgium) to obtain the morphological parameters of the subchondral bone on both medial and lateral sides. The scanning parameters included a voxel size of 18 μm , voltage of 70 kV and beam filter of 0.5 mm aluminum. After scanning, the knee joint was three-dimensionally reconstructed by NRecon software (NRecon, Bruker, Luxembourg, Belgium). BMD and the thickness of the subchondral plate (SP) were measured and calculated using CTAn software (CTAn, Bruker, Luxembourg, Belgium). For ST, a cubic ROI beneath the ROI of the SP was selected to calculate the BMD (g cm^{-3}), bone volume fraction (BV/TV, %), trabecular thickness (Tb.Th, μm), trabecular separation (Tb.Sp, μm) and trabecular number (Tb.N, $1 \mu\text{m}^{-1}$). In addition, the joint space width (JSW) between the medial femoral condyle and the medial tibial plateau was measured by CTAn software (Hellio & Mazucca, 2009). Then, three operators followed the standard image processing protocol. The reproducibility of each parameter was determined using the coefficient of variation (%) as described by Glueer et al. (1995).

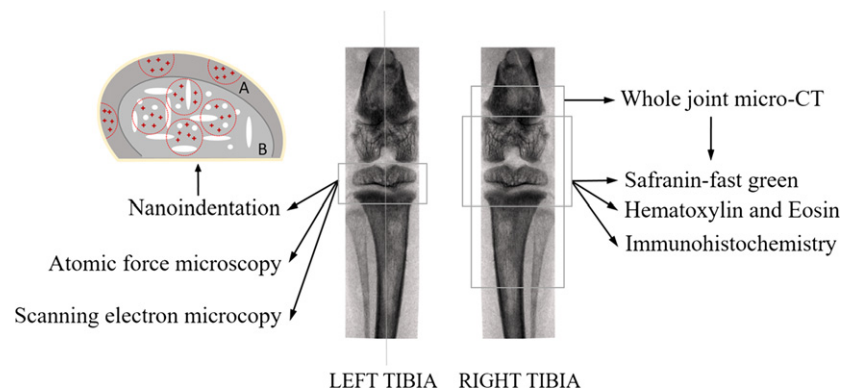


Fig. 1 Synopsis of site-specific measurements performed in the tibial articular cartilage (AC) and subchondral bone regions, and sketch map of indentation areas and sites in sagittal plane of knee joints. Considering the structural differences between subchondral plate (SP) and trabecular bone, the outer edge of the sample was set as a reference. According to the sample size, three–five semi-circles with 0.5 mm diameter were selected as indentation areas of SP (A), and three–five circles with 0.8 mm diameter were selected as indentation areas of trabecular bone (B). The red crosses in the sketch map were indentation sites, and three–five indentation sites were selected in each indentation area. Indentation sites were dispersedly distributed in each indentation area to ensure that locations of bone tissue can be selected as much as possible for the nanoindentation test; besides, the indentation sites should be far away from the edge in order to diminish the influence of embedding on the results.

Histomorphometric analysis of the ultrastructure of knee joints

After XMT scanning, knee joints were still fixed in 4% PFA for 3 days and decalcified in 10% ethylene diamine tetraacetic acid (EDTA) solution at 4 °C for 4–5 weeks. The samples were then dehydrated and embedded in paraffin by the standard method. Twelve serial sections were analyzed from each mid-medial tibial plateau in the sagittal plane, and alternately stained with hematoxylin and eosin (HE) and Safranin Orange-Fast Green. To analyze the ultrastructure of the subchondral bone, ratios of pore area/total area at the osteochondral junction and bone area/total area of the ST were quantified to represent the ultrastructure of the SP and ST, respectively (Otsuki et al. 2008). For histomorphometric analysis of the tibial cartilage, sGAG integrated optical density (IOD) was calculated (Martin et al. 1999). Optical density (OD) is defined as the logarithm of the ratio of incident to transmitted radiant power through a material, which is verified to be equal to absorbance. IOD is defined as the sum of the ODs of the individual pixels within the structure of the specimen. IOD can be calculated by the following formula: $IOD = \sum OD_i$, where OD_i represents the OD of the pixel i . IOD can reflect the integrated changes in the OD and area of the measured structure, and it is proportional to the quality of the material, which reflects the relative content of the material. Additionally, the thickness of the cartilage was calculated. Twelve sections of mid-medial tibial plateau were analyzed, and the means of the six HE-stained sections and the six Safranin Orange-Fast Green-stained sections were taken as the values for the animal for HE and Safranin Orange-Fast Green, respectively. Five measurements in each image were conducted using the image analysis software Image-Pro Plus version 6.0 (Media Cybernetics, Rockville, MD, USA).

Immunohistochemistry of type II collagen

Sections were deparaffinized and washed in phosphate-buffered saline (PBS). In addition, then endogenous peroxidase activity was quenched with 5% hydrogen peroxidase in PBS for 15 min at room temperature. The sections were repaired with 0.2% trypsin (Sigma T9935, Sigma Aldrich, St Louis, MO, USA) at 37 °C for 5 min. After natural cooling and several additional washes in PBS, the sections were immersed in 10% normal goat serum (Invitrogen, Carlsbad,

CA, USA). The sections were then incubated in a moisture chamber for 20 min at 37 °C and incubated overnight in a humid chamber at 4 °C with primary antibody rabbit polyclonal IgG of type II collagen (Abcam, Cambridge, UK). On the second day, after washing in PBS, the sections were incubated with rabbit polyclonal secondary antibody (Abcam, Cambridge, UK) for 20 min at 37 °C. The sections were visualized by reaction with diaminobenzidine (DAB) substrate. Images were captured by a microscope at 200 × magnification.

Measurements of indentation modulus and hardness using nanoindentation tests

Subchondral bone samples cut 1 mm thick from the left tibia along the median sagittal plane were used for nanoindentation tests. The samples were dehydrated in graded ethanol solutions (80–100%). All samples were embedded in epoxide resin (Epo-Thin low-viscosity epoxy; Buehler, Lake Bluff, IN, USA). All the embedded samples were metallographically polished using silicon carbide abrasive papers of decreasing grit size (300, 800, 1000, 5000 and 7000 grit). Nanoindentation tests were performed using Nano Indenter (Nano G200, Agilent Technologies, Palo Alto, CA, USA). A sharp Berkovich diamond indenter, a three-sided pyramid with an angle of 76°54' between the edges, was used for all measurements. The elastic modulus (E) and hardness (H) were determined using the method of Oliver & Pharr (1992).

All indents were made at the center of the samples based on the optical microscopy observations to eliminate any local effects. The sketch map of indentation areas and sites is shown in Fig. 1.

SEM analyses of the microarchitectural features of the surface of the ST

Subchondral bone samples cut 1 mm thick from the left tibia along the sagittal plane were used for SEM analysis. Specimens broken in half lengthwise were mounted on aluminum sample holders and sputter-coated with a thin layer of gold-platinum. Microarchitectural features of the ST surface were observed using SEM (JSM-5600 LV, JEOL, Akishima, Tokyo, Japan) in the secondary electron (SE) mode at an accelerating voltage of 8 kV. SEM images of the fracture surface were captured and compared at a magnification of 550 ×.

AFM analysis of surface characterization

Left tibias were dehydrated in graded ethanol solutions (85%, 90%, 95% and 100%, each for 2 h). Specimens (1 mm thick) were cut along the sagittal plane of the left tibial plateau by using a low-speed diamond saw. Each sample was placed horizontally onto the sample disk and imaged by AFM (Agilent 5500, Agilent Technologies, USA). Images of the cartilage, SP and ST were obtained in standard AFM tapping mode. Commercial silicon AFM probes (Tap300AL-G, Budget Sensors Instruments, Sofia, Bulgaria) with a 125 μm cantilever length, 40 Nm^{-1} constant force, 300 kHz resonant frequency and tip radius lower than 10 nm were used for analysis of the SP and trabecular bone samples, whereas probes (Tap150AL-G, Budget Sensors Instruments, Sofia, Bulgaria) with a 125 μm cantilever length, 5 Nm^{-1} constant force, 150 kHz resonant frequency and tip radius lower than 10 nm were used for analysis of the cartilage samples.

Nine locations were analyzed per sample, and $5 \times 5 \mu\text{m}$ images were acquired. Roughnesses of the cartilage, SP and ST were measured using PicoView version 1.14.4 (PicoView, Agilent Technologies, Palo Alto, CA, USA) by using the method described by Milovanovic et al. (2011).

Statistical analysis

All data were processed to obtain the medians and quartiles of all mechanical and morphological parameters of 1-, 3-, 5-, 7-, 9-, 11-, 13-, 15-, 16- and 17-month-old rats. Because the sample size is small ($n = 10$), Kruskal–Wallis H test of K independent sample non-parametric test was used to assess the differences of all age groups. The Nemenyi test of two independent samples was used to determine the differences between all the biochemical, mechanical and morphological parameters between every two groups. The statistical power analysis, which was performed by G*Power software (G*Power, Germany) when the study was planned, was 85% with the sample size of 10 and the significance criterion (α) of 0.05, and the effect size is 0.80 (Faul et al. 2007). Linear or polynomial regression analyses were performed to obtain correlations between animal age and morphological, mechanical and biochemical properties in AC and subchondral bone. Interrelations between cartilage parameters (cartilage thickness and cartilage biochemical properties) and SP parameters were analyzed using Pearson's correlation analysis. The coefficients of determination were reported as the squares of the Pearson's correlation coefficient (r^2). The use of different regression models was justified by heteroscedasticity tests and no transformations of variables were used. The selection of the final regression form (linear, exponential or logarithmic) depends on the coefficients of determination. For the piece-wise linear models, the points at which the relationships diverged were identified based on data-based considerations. Data analysis was performed with SPSS 20.0 software (SPSS Statistics 20.0, IBM, Armonk, NY, USA), and a P -value < 0.05 was considered to be significant.

Results

BMD and thickness of the tibial SP were correlated with animal age

Figure 2 shows typical XMT images and alterations of the BMD and thickness of the tibial SP of 1-, 3-, 5-, 7-, 9-, 11-, 13-, 15-, 16- and 17-month-old rats. The variations in medial and lateral BMD with age were biphasic (Fig. 2K,L). In the

first phase (1–9 months of age), medial and lateral BMD increased linearly by 3.1% and 3.7% per month, respectively, and the correlation between animal age and medial BMD ($r^2 = 0.667$, $P < 0.001$) was weaker than that of age and lateral BMD ($r^2 = 0.7486$, $P < 0.001$). In the second phase (11–17 months of age), medial and lateral BMD increased linearly by 4.2% and 3.3% per month until 17 months, respectively ($P < 0.001$). In addition, medial BMD was much higher than lateral BMD in the second phase. The variations in medial and lateral thickness with age are showed in Fig. 2M,N. The thickness of the tibial SP increased logarithmically with animal age ($P < 0.001$). The reproducibility study showed that the measurements of the BMD and thickness of the tibial SP were smaller than 6%.

BMD and microarchitectural parameters of the tibial ST were correlated with animal age

Figure 3 shows typical XMT micro-computed tomography (CT) images and changes in the BMD and microarchitecture parameters of the tibial ST from 1-, 3-, 5-, 7-, 9-, 11-, 13-, 15-, 16- and 17-month-old rats. The variations in the medial and lateral BMD with age were biphasic (Fig. 3K,L). In the first phase (1–9 months of age), medial and lateral BMD increased linearly by 1.9% and 2.1% per month, respectively, and the correlations with animal age were significant ($r^2 = 0.5749$, $P < 0.001$ and $r^2 = 0.5821$, $P < 0.001$, respectively). In the second phase (11–17 months of age), medial and lateral BMD increased linearly by 3.9% and 3.5% per month until 17 months, respectively ($P < 0.001$). Medial and lateral BV/TV (Fig. 3M,N) showed biphasic patterns similar to the BMD data. In the first phase (1–9 months of age), medial and lateral BV/TV grew logarithmically with animal age ($P < 0.001$), and they increased exponentially in the second phase (11–17 months of age; $P < 0.001$).

Linear regression analysis showed that medial and lateral Tb.Th increased linearly by approximately 6.67% and 6.37% per month until 17 months, respectively ($P < 0.001$; Fig. 3O, P), whereas medial and lateral Tb.Sp decreased exponentially (Fig. 3Q,R).

Figure 3S,T shows the variation in medial and lateral Tb.N with animal age, which exhibited biphasic behaviors. In the first phase (1–9 months of age), medial and lateral Tb.N increased linearly by 8.78% and 8.56% per month, respectively, and the correlation between animal age and variation in medial Tb.N ($r^2 = 0.8492$, $P < 0.001$) was stronger than that of age and lateral Tb.N ($r^2 = 0.7506$, $P < 0.001$). In the second phase (11–17 months of age), medial and lateral Tb.N decreased slightly.

Joint space width decreased exponentially until 17 months ($P < 0.001$; Fig. 3U).

The reproducibility studies showed that the errors in the measurements of the BMD, BV/TV, Tb.Th, Tb.N and thickness of the tibial SP were smaller than 6%.

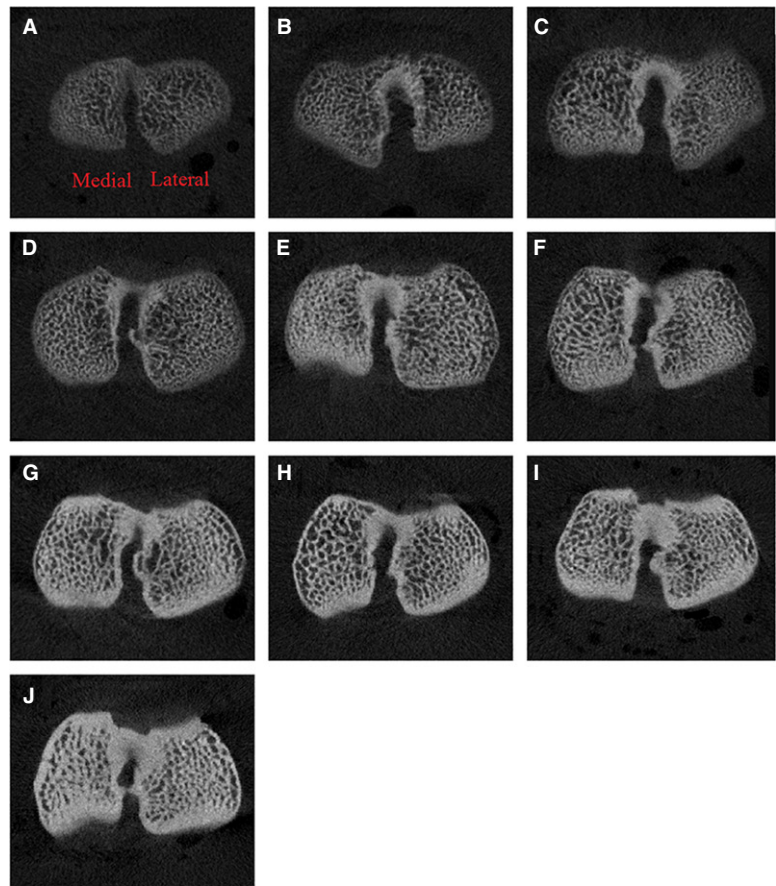
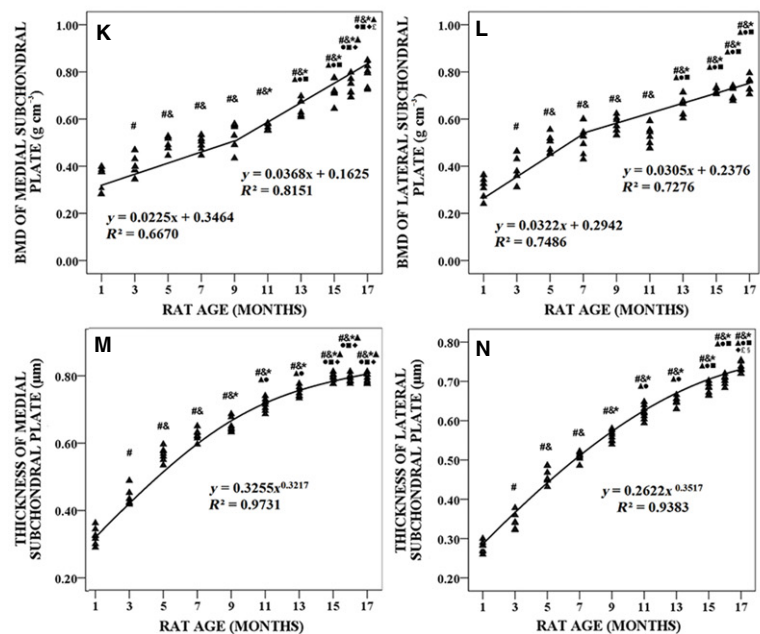


Fig. 2 Typical X-ray micro-tomography (XMT) images, bone mineral density (BMD) and thickness of tibial subchondral plate (SP) from 1-, 3-, 5-, 7-, 9-, 11-, 13-, 15-, 16- and 17-month-old rats ($n = 100$). (A–J) Typical XMT images from 1-, 3-, 5-, 7-, 9-, 11-, 13-, 15-, 16- and 17-month-old rats, respectively. (K) Medial BMD was plotted with animal age. (L) Lateral BMD was plotted with animal age. (M) Medial thickness was plotted with animal age. (N) Lateral thickness was plotted with animal age. # $P < 0.05$, compared with 1-month group; $^{\&}$ $P < 0.05$, compared with 3-month group; * $P < 0.05$, compared with 5-month group; \blacktriangle $P < 0.05$, compared with 7-month group; \bullet $P < 0.05$, compared with 9-month group; \blacksquare $P < 0.05$, compared with 11-month group; \blacklozenge $P < 0.05$, compared with 13-month group; ‡ $P < 0.05$, compared with 15-month group; § $P < 0.05$, compared with 16-month group.



Microarchitectural parameters of osteochondral were correlated with animal age

Morphological changes in the knee joint were observed by HE staining (Fig. 4A–J). Linear regression analysis showed

that the pore area/total area ratio decreased linearly by approximately 15.21% per month until 17 months ($P < 0.001$; Fig. 4L), whereas the ratio of bone area/total area increased linearly by approximately 7.79% per month until 17 months ($P < 0.001$; Fig. 4M).

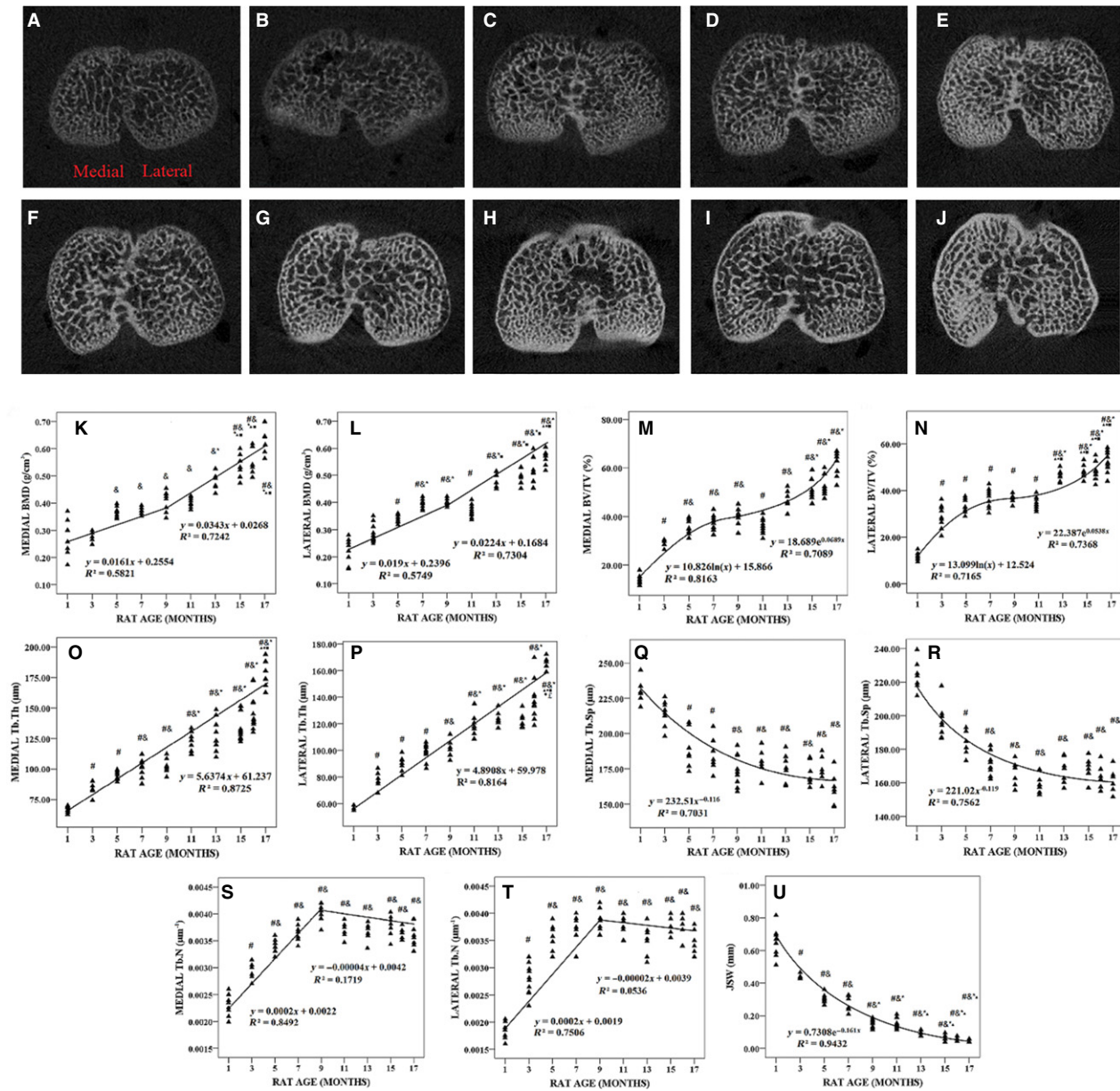


Fig. 3 Typical X-ray micro-tomography (XMT) images, bone mineral density (BMD) and microarchitecture parameters of tibial subchondral trabecular bone (ST) from 1-, 3-, 5-, 7-, 9-, 11-, 13-, 15-, 16- and 17-month-old rats ($n = 100$) and joint space width (JSW). (A–J) Typical XMT images from 1-, 3-, 5-, 7-, 9-, 11-, 13-, 15-, 16- and 17-month-old rats, respectively. (K) Medial BMD was plotted with animal age. (L) Lateral BMD was plotted with animal age. (M) Medial BV/TV was plotted with animal age. (N) Lateral BV/TV was plotted with animal age. (O) Medial Tb.Th was plotted with animal age. (P) Lateral Tb.Th was plotted with animal age. (Q) Medial Tb.Sp was plotted with animal age. (R) Lateral Tb.Sp was plotted with animal age. (S) Medial Tb.N was plotted with animal age. (T) Lateral Tb.N was plotted with animal age. (U) JSW was plotted with animal age. # $P < 0.05$, compared with 1-month group; $\text{3}P < 0.05$, compared with 3-month group; * $P < 0.05$, compared with 5-month group; $\blacktriangleup P < 0.05$, compared with 7-month group; $\bullet P < 0.05$, compared with 9-month group; $\blacksquare P < 0.05$, compared with 11-month group; $\blacklozenge P < 0.05$, compared with 13-month group; $\blacktriangleleft P < 0.05$, compared with 15-month group.

sGAG content and thickness of AC varied with age

As seen from Safranin O-Fast Green staining, there were obvious changes in the composition of AC with age (Fig. 5A–J). Figure 5K,L shows the variations in sGAG IOD

and thickness of AC with animal age, and the variations were biphasic. In the first phase (1–9 months of age), sGAG IOD and thickness of AC decreased linearly by 2.55% and 2.98% per month, respectively, and the correlation between animal age and sGAG IOD ($r^2 = 0.7558$, $P < 0.001$)

was stronger than that of age and AC thickness ($r^2 = 0.6851$, $P < 0.001$). In the second phase (11–17 months of age), sGAG IOD and thickness of AC increased slightly. The correlations between sGAG IOD, thickness of AC, thickness of the medial SP and ratio of pore area/total area at the osteochondral junction were highly significant (Table 1).

Distribution of collagen II

Collagen II was present throughout all zones of AC in each age group (Fig. 6A–J). Staining was weak with animal age, and the staining was more obvious in the middle zone. In addition, strong pericellular and interterritorial staining in the superficial and transitional zones was observed in the younger animals.

Indentation modulus and hardness measured by nanoindentation test

Figure 7 shows typical microarchitectural features of the surfaces of ST in the tibial plateau of 1-, 3-, 5-, 7-, 9-, 11-, 13-, 15-, 16- and 17-month-old rats detected by SEM and indentation modulus, and it shows the hardness of the SP and ST in the tibial plateau measured by the nanoindentation test. The indentation modulus (Fig. 7K,L) and hardness (Fig. 7M,N) of the SP and trabecular bone in the tibial plateau determined by the nanoindentation test were found to change with animal age. In the first phase (1–9 months of age), the indentation modulus of the SP and trabecular bone in the tibial plateau increased linearly by 7.54% and 9.95% per month, respectively ($P < 0.001$), and the hardness of the SP and trabecular bone in the tibial plateau increased linearly by 4.90% and 3.66% per month, respectively ($P < 0.001$). In the second phase, the indentation modulus and hardness of the bone tissue decreased slightly. The correlations between the indentation modulus of the SP, the thickness of AC and sGAG IOD were highly significant (Table 1).

SEM analysis of the microarchitecture features of the ST surface of the tibial plateau

Figure 7A–J shows the microarchitectural features of the ST surfaces as detected by SEM. When the animals were young (1–3 months of age), the trabecular number increased, and the trabeculae thinned with animal age, whereas collagen fibers arranged themselves in an orderly manner (Fig. 7A, B). When the bone enters maturity (5–9 months of age), the trabecular number decreased with animal age and the texture of the trabeculae became rough, and a plate-like texture was clearly observed in the bone samples (Fig. 7C–E). However, physically, the samples exhibited a mixed rod-plate texture. The collagen fibers were disordered, and some of the plate had peeled off (11–13 months of age; Fig. 7F,G). The structure of the trabecular bone gradually became disordered (15–17 months of age), and the fibers

were thinner and more fragile. A large number of small broken fibers was observed on the surface of the ST (Fig. 7H–J).

AFM analysis

The roughness of AC and the subchondral bone mineral grains in the tibial plateau varied with animal age and were biphasic (Fig. 8A,B), and the mean roughness of AC on the tibial plateau increased in a rapid linear fashion at a rate of 16.77% ($P < 0.001$) per month, whereas the roughness of the SP and trabecular bone of the tibial plateau decreased rapidly with the linear rates of 11.14% and 16.23%, respectively ($P < 0.001$). The correlation between roughness of AC and sGAG IOD was highly significant (Table 1).

Discussion

Female Wistar rats of different ages were investigated. The age-related morphological, biochemical and mechanical properties of AC and subchondral bone were measured by a multi-modal approach. The process of bone growth consists of two phases: the growth phase and the mature phase. The growth plate of the tibial plateau does not close during the lifetime of a rat. Despite the continued presence of growth plates in aged rats, longitudinal growth no longer occurs (Roach et al. 2003). The process of skeletal maturation proceeds along a trajectory adequately predicted by a Gompertzian function; moreover, the tibial length of female Sprague–Dawley rats increases until they are 225 days old (Jason et al. 2010). Thus, the selected growth phase of rat in our study is 1–9 months of age. The mature phase ranges from 11 to 17 months of age. The selection of a final regression form (linear, exponential or logarithmic) was dependent on the coefficients of determination. Different stages of growth and the growth curves obtained from previous studies were considered during the selection of the regression forms (Hughes & Tanner, 1970; Jason et al. 2010). A Gompertz function temporally describes the growth process through successive phases of rapid, decaying and asymptotic growth. With this function, iterative regressions with exponential, logarithmic and linear models are used to estimate the age at which the transition between the respective growth periods occurs (Jason et al. 2010). Therefore, appropriate models in this study were selected from linear, exponential or logarithmic models.

Age-related decreases in the thickness of uncalcified tibial AC at the mature stage and the advancement of tidemark with age were observed; this result is in good agreement with previous findings (Brommer et al. 2005; Turnhout et al. 2010; Moriyama et al. 2012). Notably, the percentage decreases in cartilage thickness (–2.98% per month) were similar to the amounts of sGAG evaluated by Safranin O-Fast Green staining (–2.55% per month) in the first phase

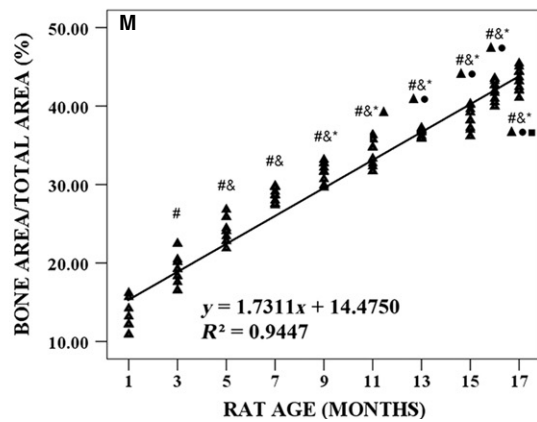
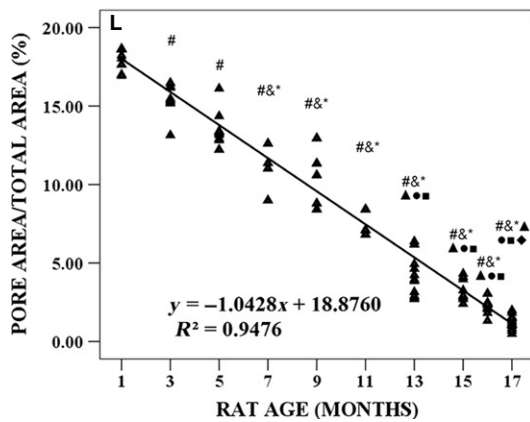
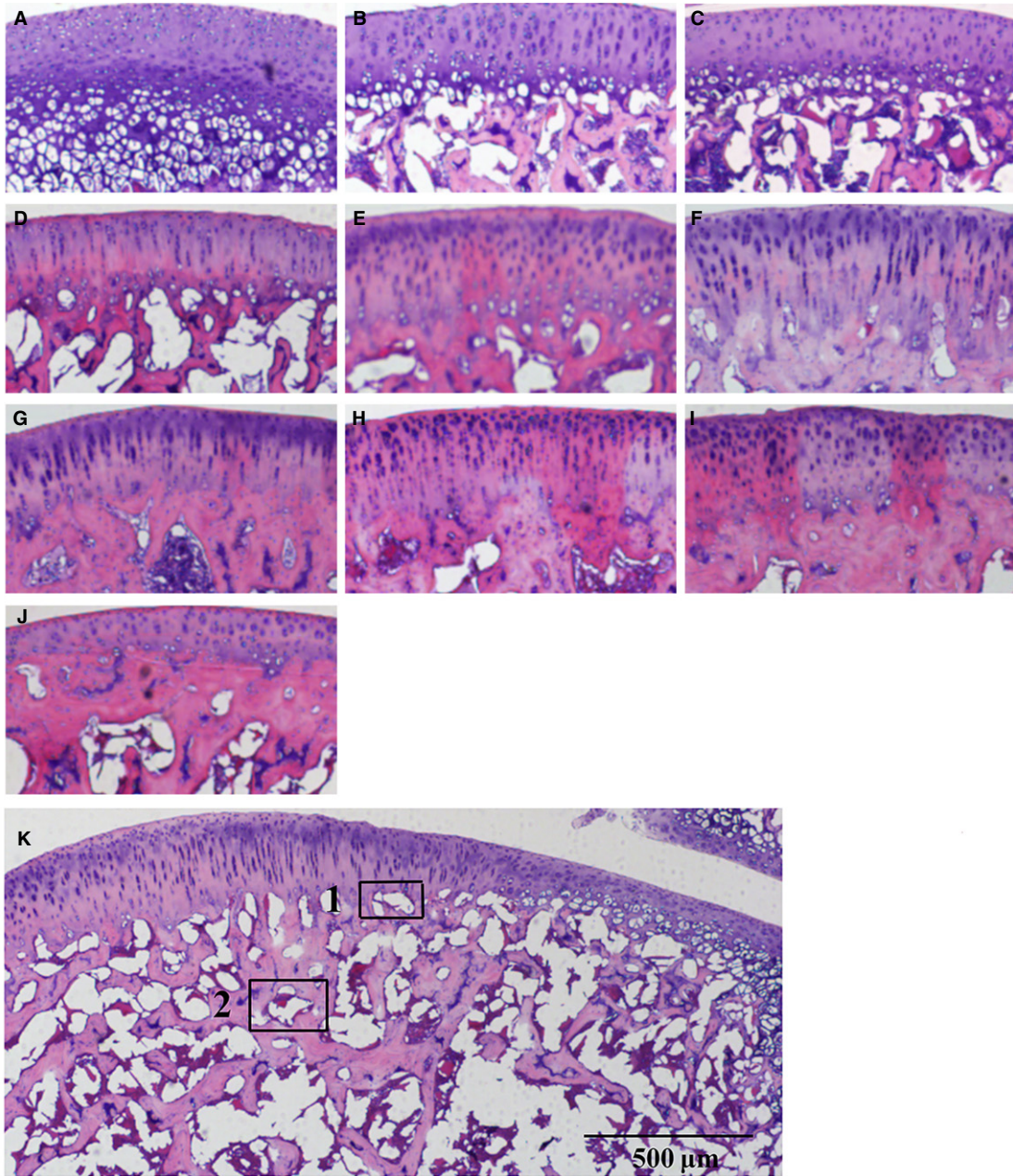


Fig. 4 Typical histology images with hematoxylin and eosin (HE) staining of articular cartilage (AC) in tibial plateau from 1-, 3-, 5-, 7-, 9-, 11-, 13-, 15-, 16- and 17-month-old rats, histological image of tibial plateau of female Wistar rats at the age of 7 months and quantitative analysis of the microarchitecture of trabecular bone in tibial plateau. (A–J) Typical histological images with HE staining from 1-, 3-, 5-, 7-, 9-, 11-, 13-, 15-, 16- and 17-month-old rats, respectively. (K) Typical image of pore area at osteochondral junction (tagged 1) and subchondral trabecular bone (ST) area of tibial plateau (tagged 2) at the age of 7 months. (L) Ratio of pore area/total area varied with animal age. (M) Ratio of bone area/total area varied with animal age. Bars represent a length of 500 μm . [#] $P < 0.05$, compared with 1-month group; [&] $P < 0.05$, compared with 3-month group; ^{*} $P < 0.05$, compared with 5-month group; [▲] $P < 0.05$, compared with 7-month group; [●] $P < 0.05$, compared with 9-month group; [■] $P < 0.05$, compared with 11-month group; [◆] $P < 0.05$, compared with 13-month group.

(1–9 months of age). This result is likely because sGAG is the major constituent of cartilage.

Growth may lead to topographical variations of AC (Hamann et al. 2014). To clarify this speculation, we performed AFM analyses. The results showed that cartilage roughness increased with age, but the amounts of sGAG in the first phase (1–9 months of age) decreased. The results of our correlation analyses showed that cartilage roughness correlates negatively with the amount of sGAG ($r = -0.68$, $P < 0.01$), which led us to speculate that the roughness of AC might be influenced by the amount of sGAG in AC. Due to the uniform staining pattern of sGAG in cartilage of all age groups, it is difficult to estimate the amount of sGAG in the superficial zone. We cannot conclude that the increase in cartilage roughness is mainly due to the decrease in sGAG. Denatured type II collagen was observed in the superficial zone of human articular femoral condylar cartilage, indicating that damage to type II collagen in aging starts at the articular surface (Hollander et al. 1995). Additionally, collagen fibrils of older mice appeared thicker on the AC surface of the femoral heads of C57BL/6 mice (Stolz et al. 2009). Thus, cartilage roughness seems to be influenced by age-related changes in collagen II. Nevertheless, the opposite has also been seen; type II collagen is lacking in the surface of pig femoral groove cartilages (age 6 months) as observed by SEM (Fujioka et al. 2013). Notably, the regions and species mentioned above are different from those in our study. The superficial collagen content of AC from different anatomical sites or species varies (Laasanen et al. 2005; Turnhout et al. 2010). Whereas pig femoral groove cartilages were investigated in that study (Fujioka et al. 2013), we analyzed tibial cartilage, which likely differs with respect to their type II collagen content and therefore roughness.

As a functional unit, AC and the subchondral bone interact with each other in the knee. The health and integrity of the overlying AC depends on the mechanical properties of the underlying subchondral bone (Lories & Luyten, 2011; Hamann et al. 2013). The AC thickness decreased considerably; the condensation of SP and ST bone within a normal rat knee in relation to developmental status was also observed. This result is in accordance with those of a previous study (Hamann et al. 2014). The ST bone is believed to deliver nutrients to the adjacent cartilage through its capillaries, which need to pass the SP (Malinin & Ouellette, 2000). This function seems to be limited by the

condensation and thickening of SP, which further changes the contents of collagen II or sGAG in AC. Our results revealed strong correlations among the contents of sGAG in AC, thickness of medial SP and ratio of pore area/total area at the osteochondral junction. This result suggests that the microarchitecture of SP may influence the composition of AC.

Increases in the indentation modulus and hardness of SP and ST bone in the first phase (1–9 months of age) were also observed in our study; these increases are associated with the changes in bone mineral content and organization (Brama et al. 2002; Hamann et al. 2013; Zuo et al. 2016). Moreover, condensation of SP may result in nanostructural changes in the mineral grains, which probably accounts for changes in the mechanical properties of subchondral bones (Brama et al. 2002). Correlations between the content of sGAG in AC and indentation modulus of SP were highly significant in our study. sGAG and collagens are responsible for the mechanical properties of AC. Therefore, the mechanical properties of AC may be affected by the mechanical properties and structure of the underlying subchondral bone. However, the AC aggregate modulus (compressive modulus) decreased during growth, which was weakly correlated with alterations in its underlying subchondral bone structure (seen by comparing 7-week-old and 13-week-old female Sprague–Dawley rats; Moriyama et al. 2012). This may be because the mechanical properties of the AC do not increase linearly during development, thereby indicating that they are highly dependent on the developmental stage and the time at which they are investigated (Julkunen et al. 2009). Hence, the mechanical properties of AC and those of subchondral bone should be investigated simultaneously across a full range of ages to fully understand the interaction between the two structures. Unfortunately, mechanical testing of AC could not be performed in our study because AC was destroyed during sample preparation for nanoindentation testing of the subchondral bone.

This study also had a few limitations. First, the samples were dehydrated in a series of graded ethanol solutions prior to the AFM observation. These dehydrated samples were different from fresh samples. The contribution of the hydrated extracellular matrix (ECM) to the actual surface roughness was neglected when measuring the surface properties of dehydrated cartilage. Although the surface roughness may be affected to some extent, all samples were

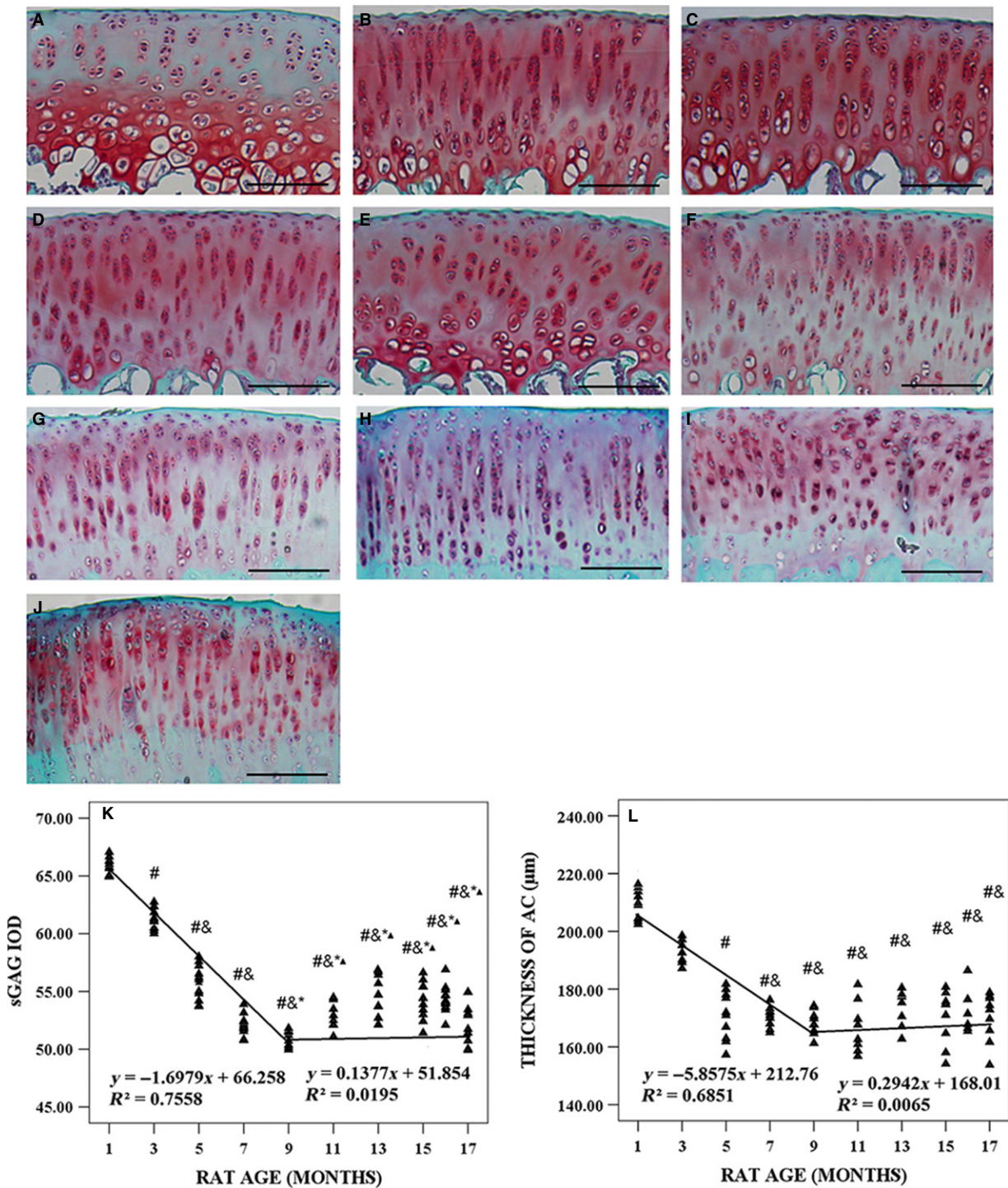


Fig. 5 Typical histology images with Safranin O-Fast Green of articular cartilage (AC) in tibial plateau from 1-, 3-, 5-, 7-, 9-, 11-, 13-, 15-, 16- and 17-month-old rats and microarchitecture parameters of AC in tibial plateau. (A–J) Typical histology images with Safranin O-Fast Green from 1-, 3-, 5-, 7-, 9-, 11-, 13-, 15-, 16- and 17-month-old rats, respectively. (K) Sulfated glycosaminoglycan (sGAG) integrated optical density (IOD) varied with animal age. (L) Thickness of AC varied with animal age. Bars represent a length of 100 µm. #*P* < 0.05, compared with 1-month group; &*P* < 0.05, compared with 3-month group; **P* < 0.05, compared with 5-month group; ▲*P* < 0.05, compared with 7-month group.

treated with the same processing procedures, and thus all experimental results were acquired under the same conditions. In addition, a previous report showed that AFM is

suitable for measuring the surface roughness of cartilage after ethanol dehydration (Ghosh et al. 2013). In our future studies, a multi-modal approach on fresh samples will be

Table 1 The correlation coefficients between all biochemical, mechanical and morphological parameters of SP and AC.

R		SP					AC		
		Med. BMD	Med.Th	Ratio	Modulus	Hardness	sGAG IOD	Thickness	Roughness
AC	sGAG IOD	-0.46*	-0.71*	0.67*	-0.54*	-0.43*	1	0.72*	-0.68*
	Thickness	-0.49*	-0.68*	0.64*	-0.52*	-0.47*	0.72*	1	-0.64*
	Roughness	0.34*	0.64*	-0.60*	0.64*	-0.50*	-0.68*	-0.64*	1

AC, articular cartilage; IOD, integrated optical density; Med. BMD, bone mineral density of medial SP; Med.Th, thickness of medial subchondral plate; Ratio, ratio of pore area/total area; sGAG, sulfated glycosaminoglycan; SP, subchondral plate.

* $P < 0.01$.

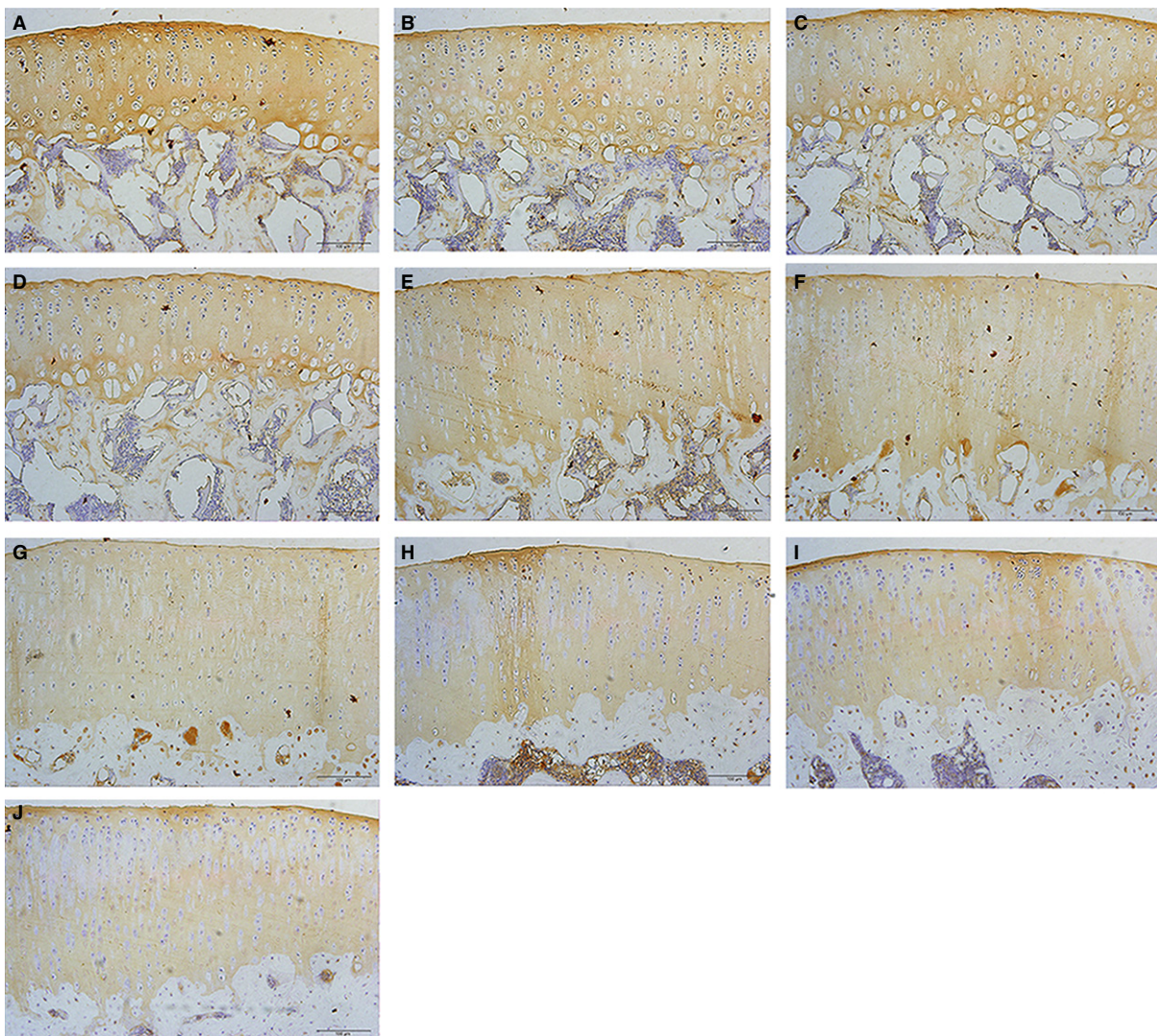


Fig. 6 Immunohistochemistry images of collagen II expression of articular cartilage (AC) in tibial plateau from 1-, 3-, 5-, 7-, 9-, 11-, 13-, 15-, 16- and 17-month-old rats. (A–J) Typical immunohistochemistry images of collagen II expression of AC in tibial plateau from 1-, 3-, 5-, 7-, 9-, 11-, 13-, 15-, 16- and 17-month-old rats, respectively. Bars represent a length of 100 μm .

carried out for actuality. The contribution of hydrated ECM to the surface properties will also be further investigated. Second, the animals in this study were purchased at full-

term age for multi-level experiments. The OARSI score was not designed in the experimental procedures to assess cartilage degeneration semi-quantitatively. In future studies,

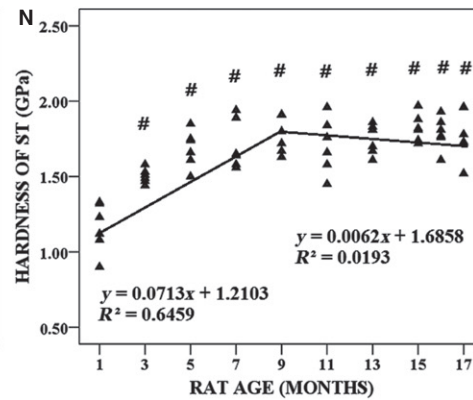
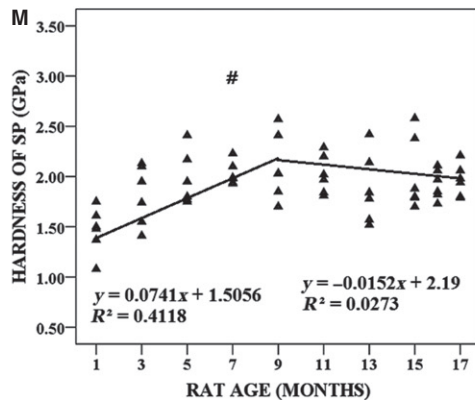
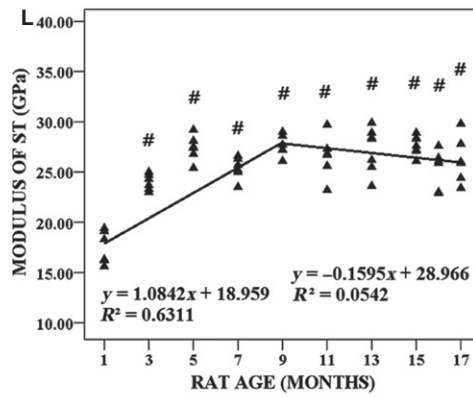
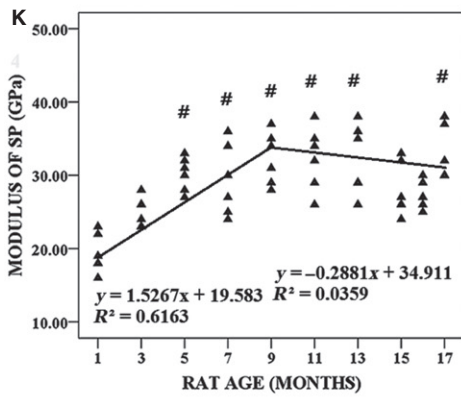
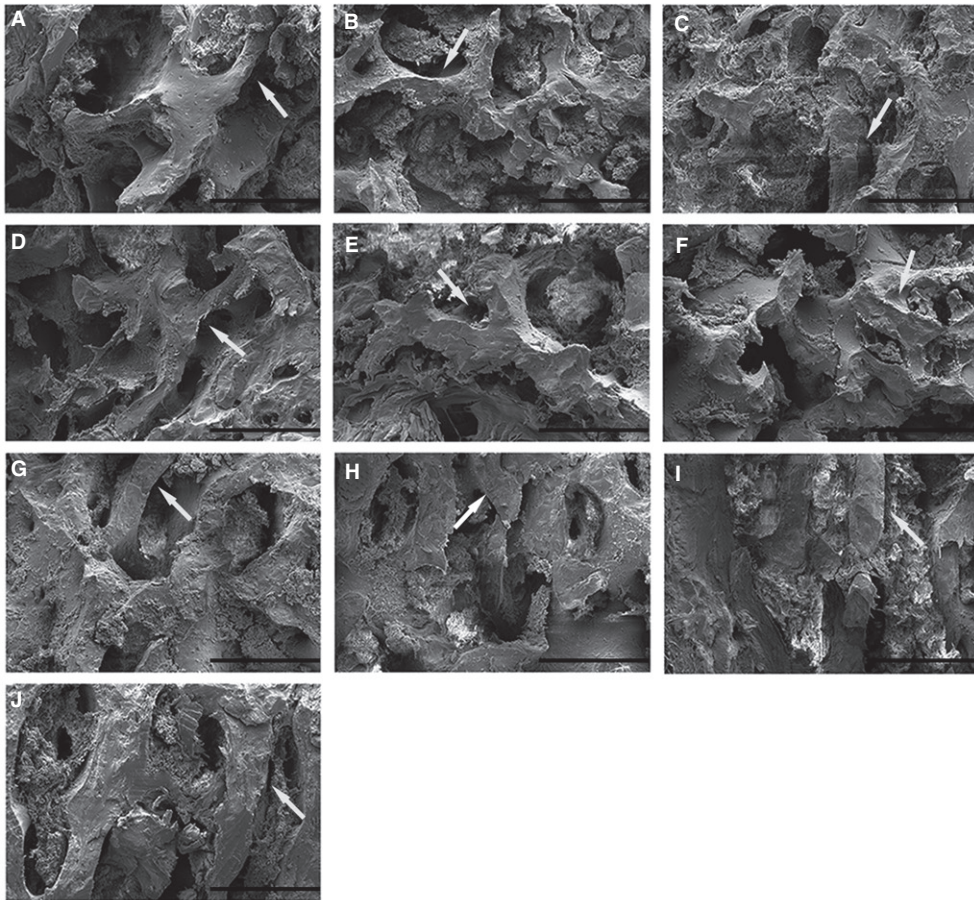


Fig. 7 Typical microarchitecture features of the surfaces of subchondral trabecular bone (ST) in tibial plateau from 1-, 3-, 5-, 7-, 9-, 11-, 13-, 15-, 16- and 17-month-old rats detected by scanning electron microscopy (SEM) and indentation modulus and hardness of subchondral plate (SP) and ST in tibial plateau measured by nanoindentation test ($n = 100$). (A–J) Typical SEM images of the surfaces of ST in tibial plateau from 1-, 3-, 5-, 7-, 9-, 11-, 13-, 15-, 16- and 17-month-old rats, respectively. Bars represent a length of 300 μm . The white arrows indicate age-related changes of ST. (K) The indentation modulus of SP in tibial plateau was plotted with animal age. (L) The indentation modulus of ST in tibial plateau was plotted with animal age. (M) The hardness of SP in tibial plateau was plotted with animal age. (N) The hardness of ST in tibial plateau was plotted with animal age. $\#P < 0.05$, compared with 1-month group.

the OARSI score will be designed to analyze age-dependent cartilage degeneration semi-quantitatively. Third, the reaction on the DAB substrate was catalyzed by peroxidase to produce water-insoluble brown material to develop the color. The OD was calculated through microscope observations and imaging analysis to determine the content. Moreover, the DAB concentration, pH, primary antibody

concentration, secondary antibody concentration and binding time in the immunohistochemical process of type II collagen were the same in this study. Thus, the experimental error was small. The brown material in the reactants can be used to locate and semi-quantitatively analyze the content of collagen II. Given that the immunohistochemistry of collagen II cannot be used to quantitatively analyze the

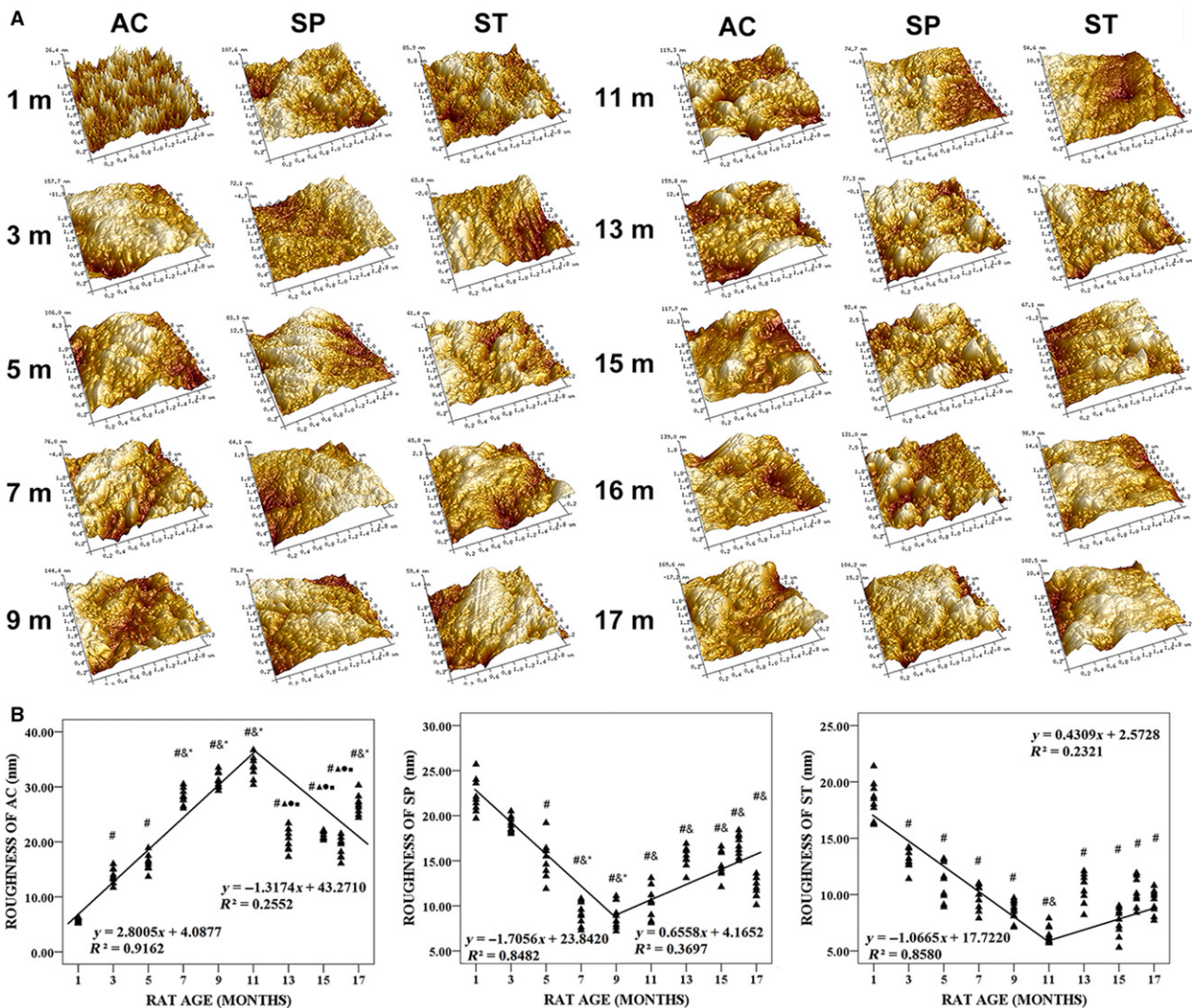


Fig. 8 Typical atomic force microscopy (AFM) topographic images (5 × 5 μm) and roughness of articular cartilage (AC) in tibial plateau, subchondral plate (SP) and subchondral trabecular bone (ST) from 1-, 3-, 5-, 7-, 9-, 11-, 13-, 15-, 16- and 17-month-old rats. (A) AFM topographic images varied with animal age. (B) Roughness varied with animal age. $\#P < 0.05$, compared with 1-month group; $\&P < 0.05$, compared with 3-month group; $*P < 0.05$, compared with 5-month group; $\blacktriangle P < 0.05$, compared with 7-month group; $\bullet P < 0.05$, compared with 9-month group; $\blacksquare P < 0.05$, compared with 11-month group.

content of collagen II, a remarkably convincing approach is needed in future studies to analyze the content of this substance quantitatively. Fourth, the samples were dehydrated during histomorphometric analysis, which consequently affected cartilage thickness. Although cartilage commonly shrinks during ethanol dehydration in histochemical processing, all the samples were treated with the same processing procedures. Furthermore, histological methods have been used to measure cartilage thickness in many studies (O'Connor, 1997; Nomura et al. 2017). In our future studies, other methods for measuring cartilage thickness will be used to obtain a result close to the true value. The effect of ethanol dehydration on cartilage thickness will also be further investigated.

In summary, a multi-modal approach was used to characterize the changes in the morphological, biochemical and mechanical properties of tibial AC and subchondral bone of female rats of different ages. Age-related changes in AC and bone properties changing among multi-levels will provide a theoretical basis for clinical research on age-related bone diseases.

Acknowledgement

The authors would like to thank Dr Jie Yao for giving advice during microarchitectural analyses.

Author contributions

All authors have made substantial contributions to study design, analysis and interpretation of data, drafting of the manuscript, and editing, making important intellectual contributions to the content of this article.

Role of the funding source

This work was supported by the National Natural Science Foundation of China (Nos 81471753, 11432016, 31570945, 11421202 and 11322223) and National Key Research and Development Program (No. 2016YFB1101101).

Competing interests

The authors declare that they have no competing interests.

References

Armstrong CG, Mow VC (1982) Variations in the intrinsic mechanical properties of human articular cartilage with age, degeneration, and water content. *J Bone Joint Surg* **64**, 88–94.

Bae WC, Temple MM, Amiel D, et al. (2003) Indentation testing of human cartilage: sensitivity to articular surface degeneration. *Arthritis Rheum* **48**, 3382–3394.

Bijlsma JWJ, Berenbaum F, Lafeber FPJG (2011) Osteoarthritis: an update with relevance for clinical practice. *The Lancet* **377**, 2115–2126.

Brama PAJ, Tekoppele JM, Bank RA, et al. (2000) Functional adaptation of equine articular cartilage: the formation of regional biochemical characteristics up to age one year. *Equine Vet J* **32**, 217–221.

Brama PAJ, Tekoppele JM, Bank RA, et al. (2002) Biochemical development of subchondral bone from birth until age eleven months and the influence of physical activity. *Equine Vet J* **34**, 143–149.

Brommer H, Brama PAJ, Laasanen MS, et al. (2005) Functional adaptation of articular cartilage from birth to maturity under the influence of loading: a biomechanical analysis. *Equine Vet J* **37**, 148–154.

Burr DB, Radin EL (2003) Microfractures and microcracks in subchondral bone: are they relevant to osteoarthritis? *Rheum Dis Clin N Am* **29**, 675–685.

Carames B, Taniguchi N, Seino D, et al. (2012) Mechanical injury suppresses autophagy regulators and its pharmacological activation results in chondroprotection. *Arthritis Rheum* **64**, 1182–1192.

Ding M (2010) Microarchitectural adaptations in aging and osteoarthrotic subchondral bone issues. *Acta Orthop* **81**, 1–53.

Ding M, Odgaard A, Linde F, et al. (2002) Age-related variations in the microstructure of human tibial cancellous bone. *J Orthop Res* **20**, 615–621.

Faul F, Erdfelder E, Lang AG, et al. (2007) G* Power 3: a flexible statistical power analysis program for the social, behavioral, and biomedical sciences. *Behav Res Methods* **39**, 175–191.

Fujioka R, Aoyama T, Takakuwa T (2013) The layered structure of the articular surface. *Osteoarthr Cartilage* **21**, 1092–1098.

Ghosh S, Bowen J, Jiang K, et al. (2013) Investigation of techniques for the measurement of articular cartilage surface roughness. *Micron* **44**, 179–184.

Glueer CC, Blake G, Lu Y, et al. (1995) Accurate assessment of precision errors: how to measure the reproducibility of bone densitometry techniques. *Osteoporosis Int* **5**, 262–270.

Guo BY, Liao DH, Li XY, et al. (2007) Age and gender related changes in biomechanical properties of healthy human costal cartilage. *Clin Biomech* **22**, 292–297.

Hamann N, Zaucke F, Dayakli M, et al. (2013) Growth-related structural, biochemical, and mechanical properties of the functional bone-cartilage unit. *J Anat* **222**, 248–259.

Hamann N, Brüggemann GP, Niehoff A (2014) Topographical variations in articular cartilage and subchondral bone of the normal rat knee are age-related. *Ann Anat* **196**, 278–285.

Hellio MP, Mazza SJ (2009) Radiographic-based grading methods and radiographic measurement of joint space width in osteoarthritis. *Radiol Clin North Am* **47**, 567–579.

Hollander AP, Pidoux I, Reiner A, et al. (1995) Damage to type II collagen in aging and osteoarthritis starts at the articular surface, originates around chondrocytes, and extends into the cartilage with progressive degeneration. *J Clin Invest* **96**, 2859–2869.

Hudelmaier M, Glaser C, Hohe J, et al. (2001) Age-related changes in the morphology and deformational behavior of knee joint cartilage. *Arthritis Rheum* **44**, 2556–2561.

Hughes PC, Tanner JM (1970) The assessment of skeletal maturity in the growing rat. *J Anat* **106**, 371.

Jason AH, Bariteau JT, Loomis RM, et al. (2010) Ontogeny of skeletal maturation in the juvenile rat. *Anat Rec* **291**, 283–292.

Julkunen P, Harjula T, Iivarinen J, et al. (2009) Biomechanical, biochemical and structural correlations in immature and mature rabbit articular cartilage. *Osteoarthr Cartilage* **17**, 1628–1638.

- Kobayashi-Miura M, Miura T, Osago H, et al.** (2016) Rat articular cartilages change their tissue and protein compositions during perinatal period. *Anat Histol Embryol* **45**, 9–18.
- Laasanen MS, Saarakkala S, Töyräs J, et al.** (2005) Site-specific ultrasound reflection properties and superficial collagen content of bovine knee articular cartilage. *Phys Med Biol* **50**, 3221.
- Lau A, Oyen ML, Kent RW, et al.** (2008) Indentation stiffness of aging human costal cartilage. *Acta Biomater* **4**, 97–103.
- Li G, Yin J, Gao J, et al.** (2013) Subchondral bone in osteoarthritis: insight into risk factors and microstructural changes. *Arthritis Res Ther* **15**, 223.
- Li G, Zheng Q, Landao-Bassonga E, et al.** (2015a) Influence of age and gender on microarchitecture and bone remodeling in subchondral bone of the osteoarthritic femoral head. *Bone* **77**, 91–97.
- Li XF, Cai XR, Fan F, et al.** (2015b) Observation of sGAG content of human hip joint cartilage in different old age groups based on EPIC micro-CT. *Connective Tissue Res* **56**, 99–105.
- Loeser RF** (2009) Aging and osteoarthritis: the role of chondrocyte senescence and aging changes in the cartilage matrix. *Osteoarthr Cartilage* **17**, 971–979.
- Lories RJ, Luyten FP** (2011) The bone–cartilage unit in osteoarthritis. *Nat Rev Rheumatol* **7**, 43–49.
- Lotz M, Loeser RF** (2012) Effects of aging on articular cartilage homeostasis. *Bone* **51**, 241–248.
- Malinin T, Ouellette EA** (2000) Articular cartilage nutrition is mediated by subchondral bone: a long-term autograft study in baboons. *Osteoarthr Cartilage* **8**, 483–491.
- Maroudas A, Bayliss MT, Venn MF** (1980) Further studies on the composition of human femoral head cartilage. *Ann Rheum Dis* **39**, 514–523.
- Martin I, Obradovic B, Freed LE, et al.** (1999) A method for quantitative analysis of glycosaminoglycan distribution in cultured natural and engineering cartilage. *Ann Biomed Eng* **27**, 656–662.
- Mclauchlan GJ, Gardner DL** (2002) Sacral and iliac articular cartilage thickness and cellularity: relationship to subchondral bone end-plate thickness and cancellous bone density. *Rheumatology* **41**, 375–380.
- Milovanovic P, Potocnik J, Stoilkovic M, et al.** (2011) Nanostructure and mineral composition of trabecular bone in the lateral femoral neck: implications for bone fragility in elderly women. *Acta Biomater* **7**, 3446–3451.
- Moriyama H, Kanemura N, Brouns I, et al.** (2012) Effects of aging and exercise training on the histological and mechanical properties of articular structures in knee joints of male rat. *Biogerontology* **13**, 369–381.
- Mow VC, Ratcliffe A, Poole AR** (1992) Cartilage and diarthrodial joints as paradigms for hierarchical materials and structures. *Biomaterials* **13**, 67–97.
- Nebelung S, Brill N, Müller F, et al.** (2016) Towards optical coherence tomography-based elastographic evaluation of human cartilage. *J Mech Behav Biomed* **56**, 106–119.
- Nomura M, Sakitani N, Iwasawa H, et al.** (2017) Thinning of articular cartilage after joint unloading or immobilization. An experimental investigation of the pathogenesis in mice. *Osteoarthr cartilage* **25**, 727–736.
- O'Connor KM** (1997) Unweighting accelerates tidemark advancement in articular cartilage at the knee joint of rats. *J Bone Miner Res* **12**, 580–589.
- O'Hara BP, Urban JP, Maroudas A** (1990) Influence of cyclic loading on the nutrition of articular cartilage. *Ann Rheum Dis* **49**, 536–539.
- Oliver WC, Pharr GM** (1992) An improved technique for determining hardness and elastic modulus using load and displacement sensing indentation experiments. *J Mater Res* **7**, 1564–1583.
- Otsuki S, Brinson DC, Creighton L, et al.** (2008) The effect of glycosaminoglycan loss on chondrocyte viability: a study on porcine cartilage explants. *Arthritis Rheum* **58**, 1076–1085.
- Pearle AD, Warren RF, Rodeo SA** (2005) Basic science of articular cartilage and osteoarthritis. *Clin Sport Med* **24**, 1–12.
- Peng Z, Wang M** (2013) Three dimensional surface characterization of human cartilages at a micron and nanometre scale. *Wear* **301**, 210–217.
- Roach HI, Mehta G, Oreffo RO, et al.** (2003) Temporal analysis of rat growth plates: cessation of growth with age despite presence of a physis. *J Histochem Cytochem* **51**, 373.
- Stolz M, Gottardi R, Raiteri R, et al.** (2009) Early detection of aging cartilage and osteoarthritis in mice and patient samples using atomic force microscopy. *Nat Nanotechnol* **4**, 186–192.
- Temple MM, Bae WC, Chen MQ, et al.** (2009) Biomechanical, structural, and biochemical indices of degenerative and osteoarthritic deterioration of adult human articular cartilage of the femoral condyle. *Osteoarthr Cartilage* **17**, 1469–1476.
- Turnhout MCV, Schipper H, Engel B, et al.** (2010) Postnatal development of collagen structure in ovine articular cartilage. *BMC Dev Biol* **10**, 1–16.
- Van Turnhout MC, Haazelager MB, Gijzen MAL, et al.** (2008) Quantitative description of collagen structure in the articular cartilage of the young and adult equine distal metacarpus. *Anim Biol* **58**, 353–370.
- Wang YXJ, Griffith JF, Ahuja AT** (2010) Non-invasive MRI assessment of the articular cartilage in clinical studies and experimental settings. *World J Radiol* **2**, 44.
- Wang T, Wen CY, Yan CH, et al.** (2013) Spatial and temporal changes of subchondral bone proceed to microscopic articular cartilage degeneration in guinea pigs with spontaneous osteoarthritis. *Osteoarthr Cartilage* **21**, 574–581.
- Zuo Q, Lu S, Du Z, et al.** (2016) Characterization of nano-structural and nano-mechanical properties of osteoarthritic subchondral bone. *BMC Musculoskelet Disord* **17**, 367.